

On the accuracy of the LSC-IVR approach for excitation energy transfer in molecular aggregates

Cite as: J. Chem. Phys. **146**, 144105 (2017); <https://doi.org/10.1063/1.4979894>

Submitted: 05 January 2017 . Accepted: 24 March 2017 . Published Online: 12 April 2017

Hung-Hsuan Teh, and Yuan-Chung Cheng 



View Online



Export Citation



CrossMark

ARTICLES YOU MAY BE INTERESTED IN

[Mean-trajectory approximation for electronic and vibrational-electronic nonlinear spectroscopy](#)

The Journal of Chemical Physics **146**, 144106 (2017); <https://doi.org/10.1063/1.4979621>

[Ultrafast coherent energy transfer with high efficiency based on plasmonic nanostructures](#)

The Journal of Chemical Physics **146**, 144101 (2017); <https://doi.org/10.1063/1.4979671>

[Excited states from modified coupled cluster methods: Are they any better than EOM CCSD?](#)

The Journal of Chemical Physics **146**, 144104 (2017); <https://doi.org/10.1063/1.4979078>

Lock-in Amplifiers

Find out more today



 Zurich
Instruments

On the accuracy of the LSC-IVR approach for excitation energy transfer in molecular aggregates

Hung-Hsuan Teh and Yuan-Chung Cheng^{a)}

Department of Chemistry and Center for Quantum Science and Engineering, National Taiwan University, Taipei City 106, Taiwan

(Received 5 January 2017; accepted 24 March 2017; published online 12 April 2017)

We investigate the applicability of the linearized semiclassical initial value representation (LSC-IVR) method to excitation energy transfer (EET) problems in molecular aggregates by simulating the EET dynamics of a dimer model in a wide range of parameter regime and comparing the results to those obtained from a numerically exact method. It is found that the LSC-IVR approach yields accurate population relaxation rates and decoherence rates in a broad parameter regime. However, the classical approximation imposed by the LSC-IVR method does not satisfy the detailed balance condition, generally leading to incorrect equilibrium populations. Based on this observation, we propose a post-processing algorithm to solve the long time equilibrium problem and demonstrate that this long-time correction method successfully removed the deviations from exact results for the LSC-IVR method in all of the regimes studied in this work. Finally, we apply the LSC-IVR method to simulate EET dynamics in the photosynthetic Fenna-Matthews-Olson complex system, demonstrating that the LSC-IVR method with long-time correction provides excellent description of coherent EET dynamics in this typical photosynthetic pigment-protein complex. *Published by AIP Publishing.* [<http://dx.doi.org/10.1063/1.4979894>]

I. INTRODUCTION

Quantum dynamics involving transitions between electronic states play important roles in condensed-phase systems. There, interactions between electronic degrees of freedom and nuclear motions often govern the dynamics of electronic transitions, and a system-bath model adopting an electronic system coupled to nuclear bath modes is often used to describe the dynamics. In these cases, methodologies incorporating quantum effects while retaining favorable computational cost exhibited by evolving classical dynamics are desirable. Thus, various mixed quantum classical methods, such as the surface hopping formalism,^{1,2} the mixed quantum classical Liouville equation,^{3,4} and ring polymer molecular dynamics^{5,6} have been developed. It has been shown that these methods provide reasonable results in many model systems;^{6–8} nevertheless, shortcomings such as incomplete descriptions of feedback from bath parts to the system, instabilities in the numerical integration scheme, or restriction to the high temperature limit still hinder the applications of these approaches.

Going beyond the pure classical approximation, semiclassical (SC) methods utilize information from classical trajectories to calculate the quantum propagator.⁹ Since these approaches only require classical trajectories as the input, in principle it is possible to simulate dynamics of complex systems based on molecular dynamics simulations. In particular, the semiclassical initial value representation (SC-IVR) developed by Miller and co-workers^{10–12} provides

a solid mathematical foundation for rigorous formulation of semiclassical quantum dynamics. Moreover, for simulations of nonadiabatic dynamics that involve potential energy surfaces of multiple discrete electronic states, the Meyer-Miller-Stock-Thoss (MMST) representation can be utilized to provide an exact mapping of the electronic degrees of freedom to a set of harmonic modes to facilitate semiclassical calculations.^{13–15} Nonetheless, as one focuses on truly complex systems, the interference between the trajectories often causes computational difficulty in semiclassical descriptions. Although this problem can be largely removed by using the forward-backward IVR,^{16,17} computational cost of SC-IVR is still very high if convergent results for long-time dynamics are needed, and this has hindered the application of the full SC-IVR method to complex systems.

In order to deal with the problems in the SC-IVR method, Wang *et al.* suggested a linearized form of the propagator.¹⁸ This linearized SC-IVR (LSC-IVR) approach provides exact results in the high-temperature limit and the harmonic limit.¹⁹ Combined with the MMST mapping approach, LSC-IVR has been applied to simulate electronically nonadiabatic processes, including one-dimensional two-state scattering problems^{18,20} and spin-boson problems,^{10,21} and its shortcomings have been extensively discussed in the literature.^{12,20,22–24} Besides, it was demonstrated that the LSC-IVR approach is able to describe quantum effects in the short time dynamics ($t < \hbar\beta$) of the flux correlation functions in isomerization processes.²⁵ Wang *et al.* further demonstrated that qualitative results with important physical insights could be obtained in a spin-boson model by the LSC-IVR approach,²¹ and more recent theoretical advances of the LSC-IVR method has significantly expanded its range of applicability.^{26–28}

^{a)}Electronic mail: yuanchung@ntu.edu.tw

More recently, inspired by experiments pertaining to quantum coherence phenomena in photosynthetic light-harvesting systems,^{29–31} LSC-IVR and related approaches have been applied to investigate coherent excitation energy transfer (EET) dynamics in condensed-phase molecular systems.^{32–35} In particular, Tao and Miller have applied the LSC-IVR approach to investigate models for EET in molecular dimer systems as well as the EET dynamics in the photosynthetic Fenna-Matthews-Olson (FMO) complex to reveal the success of the linearized semiclassical approximation in these calculations,³² and novel insights about the nature of the coherent dynamics in the EET processes could be obtained from the semiclassical representation.²⁴ Specifically, Miller and co-workers have shown that while LSC-IVR could not capture nuclear quantum coherence effects due to the linearization approximation, the method correctly describes coherent evolutions of electronic populations embedded in the Meyer-Miller representation. In this regard, Miller had pointed out that the coherent electronic dynamics as often displayed in oscillatory population beatings can be described by classical coherence effects.^{24,32} These studies have demonstrated that the LSC-IVR approach is a promising method for the simulation of EET dynamics in condensed-phase molecular systems. Nevertheless, while LSC-IVR has been applied to spin-boson problems in various parameter regimes, in general the quantitative accuracy of the LSC-IVR method when applied to EET problems is still largely unclear as a comprehensive benchmark study for parameters suitable for EET problems is not available. Thus, it will be desirable to elucidate the applicability of the LSC-IVR approach in a broad parameter regime for EET processes and to improve the performance of the LSC-IVR method if possible.

In this work, we aim to examine the applicability of the LSC-IVR method to EET problems by a comprehensive benchmark against numerically exact results. This paper is organized as follows: Section II first provides a concise review of the theoretical background of the LSC-IVR method. In Sec. III, we present a comprehensive investigation of the performance of the LSC-IVR method over a wide range of EET parameters by comparing EET dynamics of a dimer model simulated using the LSC-IVR approach against the results provided by the quasi-adiabatic path integral (QUAPI)^{36,37} method. The comparison reveals applicable regimes of the LSC-IVR approach and physical insights about the drawbacks of the method. These benchmark results inspired us to propose a post-processing algorithm to improve the LSC-IVR method, and we show that the simple correction provides accurate simulations of EET dynamics in Sec. IV. Finally, in Sec. V we apply the LSC-IVR approach to describe EET dynamics in the FMO complex, demonstrating that with the aid of the simple correction algorithm proposed in this work, the LSC-IVR approach yields EET dynamics in excellent agreement with numerically exact results in this photosynthetic system.

II. THEORETICAL BACKGROUND

A. LSC-IVR

Quantum time correlation functions³⁸ play central roles in calculating physical quantities and responses in dynamical

systems. For example, the diffusion coefficient is related to the velocity-velocity time correlation function, and the absorption lineshape is related to the dipole-dipole time correlation function. The general form of a quantum time correlation function is given by ($\hbar = 1$)

$$C_{AB}(t) = \text{Tr} \left[e^{-iHt} A e^{iHt} B \right], \quad (1)$$

where A and B are the two observables and H is the Hamiltonian of the total system. $C_{AB}(t)$ provides a statistical description of the fluctuation of the time-dependent variables of a system in the thermal equilibrium.

In a semiclassical approach, the two propagators in the time correlation function are substituted by semiclassical propagators, which leads to a double integral over two initial phase space distributions. In principle, these integrals can be calculated exactly in the IVR representation^{10,11} by using, for example, the forward-backward IVR method; however, in practice these exact approaches are computationally expensive and thus limited to calculations for small systems. To deal with molecular processes in complex systems, we focus on the linearized SC-IVR method suggested by Wang *et al.*¹⁸ In this approach, the contribution to the integral is assumed to mainly come from the terms in which the differences between the positions and the momenta of the two phase space points at time zero are small enough; therefore, the expansion to the first order can be used. This leads to a simple double integral over the initial phase space,

$$C_{AB}(t) \approx \left(\frac{1}{2\pi} \right)^f \int d\bar{\mathbf{x}}_0 \int d\bar{\mathbf{p}}_0 A^W(\bar{\mathbf{x}}_0, \bar{\mathbf{p}}_0) B^W(\bar{\mathbf{x}}_t, \bar{\mathbf{p}}_t)^*, \quad (2)$$

where f is the number of the degrees of freedom and $O^W(\mathbf{x}, \mathbf{p})$ denotes the Wigner function of an operator O ,

$$O^W(\mathbf{x}, \mathbf{p}) = \int d\Delta\mathbf{x} e^{-i\mathbf{p}\Delta\mathbf{x}} \langle \mathbf{x} + \frac{\Delta\mathbf{x}}{2} | O | \mathbf{x} - \frac{\Delta\mathbf{x}}{2} \rangle. \quad (3)$$

In Equation (2), \mathbf{x}_t and \mathbf{p}_t are the classical position and momentum at time t propagated by Hamilton's equations with the initial conditions \mathbf{x}_0 and \mathbf{p}_0 , respectively. Compared to the full SC-IVR approaches, Eq. (2) can be evaluated much more easily since it only consists of one integral over the initial phase space.

B. Meyer-Miller-Stock-Thoss representation

The LSC-IVR method enables the evaluation of time correlation functions by the propagation of classical dynamics. In adiabatic processes, it is straightforward to apply the LSC-IVR to calculate the dynamics on a single electronic potential, which provides semiclassical molecular dynamics. However, in order to consider nonadiabatic processes involving two or more electronic states in the semiclassical formalism, a classical representation for discrete quantum states is required. A consistent treatment for combined electronic and nuclear degrees of freedom can be achieved using the mapping approach of Meyer, Miller, Stock, and Thoss.^{13–15}

In the Meyer-Miller-Stock-Thoss (MMST) representation, a system with N_e discrete electronic states is described by the general Hamiltonian

$$H(\mathbf{X}, \mathbf{P}) = \sum_{n,m=1}^{N_e} H_{nm}(\mathbf{X}, \mathbf{P}) |n\rangle \langle m|, \quad (4)$$

where \mathbf{X} and \mathbf{P} are the positions and the momenta of the nuclear coordinates, respectively, and $|n\rangle$ is the n th electronic state. The key concept is to map N_e discrete electronic states to the zero and one quanta space of N_e harmonic oscillators,

$$|n\rangle \rightarrow |0_1, 0_2, \dots, 0_{n-1}, 1_n, 0_{n+1}, \dots, 0_{N_e}\rangle, \quad (5)$$

where the suffixes label the electronic states, and $|0_1, 0_2, \dots, 0_{n-1}, 1_n, 0_{n+1}, \dots, 0_{N_e}\rangle$ denotes a harmonic oscillator state in which the n th oscillator is in the first vibrational excited state and all the other oscillators are in the corresponding vibrational ground states.

After recasting Eq. (4) in the second quantization form and transforming from ladder operators to momentum and position operators, the final expression of the Hamiltonian in the MMST representation can be obtained,¹⁴

$$H(\mathbf{X}, \mathbf{P})^{MMST} = \sum_n \frac{1}{2} (x_n^2 + p_n^2 - 1) H_{nn} + \sum_{m>n} (x_n x_m + p_n p_m) H_{nm}. \quad (6)$$

Equation (6) is equivalent to Eq. (4) if the dynamics are treated quantum mechanically. In this case, the propagation is confined in the mapped zero and one occupation number states of the vibrational Hilbert space since the number operator commutes with the Hamiltonian, and as a result the mapping is exact. However, when we regard the operators \mathbf{x} and \mathbf{p} as continuous classical variables, the semiclassical propagation in the mapped basis deviates from the zero- and single-excitation subspace to the complete Hilbert space, leading to errors in the dynamics. This violation of the conservation of the mapping subspace was referred to as the zero-point energy flow problem in the literature.^{22,39} In the LSC-IVR representation, the mapping is accurate only at the infinite temperature.

C. Model system

In order to investigate the applicability of the LSC-IVR method to EET problems, we follow the framework developed by Tao and Miller. In this paper, we confine ourselves to a simple EET model⁴⁰ composed of a dimer system linearly coupled to harmonic baths described by the following Hamiltonian:

$$H = H_s + H_b + H_{sb}, \quad (7)$$

where

$$H_s = \Delta \sigma_z + J \sigma_x, \quad (8)$$

and σ_z and σ_x are the Pauli matrices, 2Δ is the site energy gap, and J is the coupling between the two sites. Moreover, the bath Hamiltonian and the system-bath coupling are described by

$$H_b + H_{sb} = \sum_{i=1}^{N_b} \omega_i \left(\frac{1}{2} X_i^2 + \frac{1}{2} P_i^2 \right) + \sum_{n=1,2} \sum_i \sqrt{2} \omega_i g_{in} X_i a_n^\dagger a_n, \quad (9)$$

with ω_i and g_i the frequency of the i th bath mode and the system-bath coupling constant between the i th bath mode and the n th site, respectively. We consider a model in which the system-bath interactions are determined from a super-Ohmic spectral density, and the details will be described in Sec. II D.

In this work, we suppose that the system is initially excited on site 1, and thus the total density matrix at $t = 0$ is in a factorized product state of the form

$$\rho(0) = |1\rangle\langle 1| \otimes \rho_{eq}^b, \quad (10)$$

where $\beta = 1/k_B T$ is the inverse temperature and $\rho_{eq}^b = e^{-\beta H_b} / Z$. In general, this initial condition might not be appropriate since it neglects the correlation between the system and the bath. Nevertheless, this initial state describes the electronic excitation processes because it is in accord with the Franck-Condon approximation. Finally, note that although a harmonic system is considered here, it should be clear that a generalization to the anharmonic bath and the nonlinear system-bath coupling would not increase any additional effort in the calculation using the LSC-IVR approach.

D. Bath discretization

To model condense-phase environments, the couplings of the system to the bath can be specified by spectral density functions generally defined as

$$\mathcal{J}_{nm}(\omega) \equiv \sum_i g_{in} g_{im} \omega_i^2 \delta(\omega - \omega_i). \quad (11)$$

There, \mathcal{J}_{nn} describes the coupling of the n th pigment to the bath modes, and \mathcal{J}_{nm} ($n \neq m$) describes correlated coupling of the bath modes shared between the n th and the m th sites. Following previous works in the description of EET systems, here we study the super-Ohmic spectral density

$$\mathcal{J}_{nm}(\omega) = \delta_{nm} \gamma \frac{\omega^3}{\omega_c^2} e^{-\omega/\omega_c}, \quad (12)$$

where γ is the coupling strength and ω_c is the bath cut-off frequency. For simplicity, we assume that the baths coupled to each site to be identical and independent.

In the LSC-IVR with MMST representation, however, the dynamics of the bath should be described by a finite set of discrete bath modes. As a result, we need to find a set of discrete bath modes that best represents the spectral density. We carry out the bath discretization following the procedure of Wang *et al.*²¹ In this approach, a density of state function $W(\omega)$ that satisfies the following two conditions²¹ is introduced:

$$\int_0^{\omega_M} W(\omega) d\omega = N_b, \quad (13)$$

$$\int_0^{\omega_i} W(\omega) d\omega = i, \quad (14)$$

where N_b is the number of bath modes, i labels the i th mode with frequency ω_i , and ω_M is the largest discrete frequency of the mode modes we choose. The precise functional form of $W(\omega)$ does not affect the average results of the dynamics if a large number of bath modes are included. We have examined various forms of the $W(\omega)$, and we find that the difference among them is the number of trajectories required for achieving numerical convergences. All simulation results presented in the paper adopt the following choice of $W(\omega)$:

$$W_n(\omega) = a \frac{\mathcal{J}_{nn}(\omega)}{\omega}, \quad (15)$$

where a is a normalization constant determined by Eq. (13). With the density of state function determined, the corresponding system-bath coupling to each mode g_i can be obtained from the definition of the spectral density (Eq. (11))

$$g_i^2 = \frac{\mathcal{J}_{nn}(\omega_i)}{\omega_i^2 W(\omega_i)}. \quad (16)$$

Note that samplings of classical harmonic bath frequencies based on Eq. (15) mainly focus on the low frequency part because most contributions from the high frequency modes quickly cancel out as we take the ensemble average. All results presented in this work includes $N_b = 200$ modes and 50 000 trajectories for ensemble average, and we have numerically confirmed the convergence of all the calculations.

III. PERFORMANCE OF LSC-IVR

In this section, the accuracy of the LSC-IVR approach in simulating EET population dynamics is investigated by comparing it with the numerically exact quasi adiabatic path integral (QUAPI)^{36,37} method. To this end, we investigate the population transfer dynamics of dimer systems with different parameters (site energy gap 2Δ , electronic coupling J , system bath coupling strength γ , and temperature T) when the system is initially excited on site 1 (Eq. (10)). The parameters used here cover a broad EET parameter space and should be large enough to comprehend physics we are interested in.

Representative results of population dynamics calculated by the LSC-IVR method at various parameter regimes are depicted in Fig. 1. Figure 1(a) is a case with small energy gap ($D/\omega_c = 0.1$), small electronic coupling ($J/\omega_c = 0.5$), intermediate system-bath coupling ($\gamma = 0.2/\pi$), and high temperature ($k_B T/\omega_c = 10.0$). It is clear that the LSC-IVR method yields excellent results in this case, and this is expected since the temperature is high. In addition, the error from the approximation of the MMST representation is also negligible in this intermediate system-bath coupling regime. Figure 1(b) shows a case with same parameters as Fig. 1(a) except for a larger energy gap ($D/\omega_c = 0.5$) and lower

temperature ($k_B T/\omega_c = 2.0$). In this case, the LSC-IVR result clearly deviates from the exact result. Notice that the decoherence rate is still accurately described by the LSC-IVR approach; nonetheless, the discrepancy in the population could be observed which is due to the classical approximation imposed in this approach, leading to the incorrect equilibrium position at long times. In Fig. 1(c), we provide an example with a strong system-bath coupling ($\gamma = 2.0/\pi$) and at a low temperature ($k_B T/\omega_c = 0.5$), which is expected to cause difficulties to the LSC-IVR method. Indeed, we find a large difference between the results calculated by the LSC-IVR method and the QUAPI data in this over-damped regime. Nevertheless, we observe that the LSC-IVR approach still accurately predicts the decaying rate. Again, it is observed that the LSC-IVR dynamics incorrectly predicts the equilibrium positions. These phenomena are a key problem of LSC-IVR dynamics which is observed in a large parameter regime, demonstrating that the key pitfall of the LSC-IVR in the MMST representation approach is the violation of the detail balance.

In Fig. 2 we investigate the effect of eigen-energy gap on the accuracy of the LSC-IVR approach. The eigen-energy gap, $\Delta E = 2\sqrt{\Delta^2 + J^2}$, is the energy gap between the eigenstates of the system Hamiltonian H_s . Figures 2(a)–2(c) show dynamics of systems with the same system-bath coupling strength $\gamma = 0.5/\pi$ and temperature $k_B T/\omega_c = 0.5$, but the eigen-energy gap $\Delta E/\omega_c$ is set at 1.02, 1.41, and 2.24, respectively. If we ignore the deviations of equilibrium populations, we can observe that the LSC-IVR method yields better population beating dynamics with the increase of ΔE . In the case of small $\Delta E/\omega_c$, the LSC-IVR significantly overestimates the decoherence rate, and this is because the large numbers of high-frequency bath modes incorrectly influence the dynamics due to classical representation of these modes.

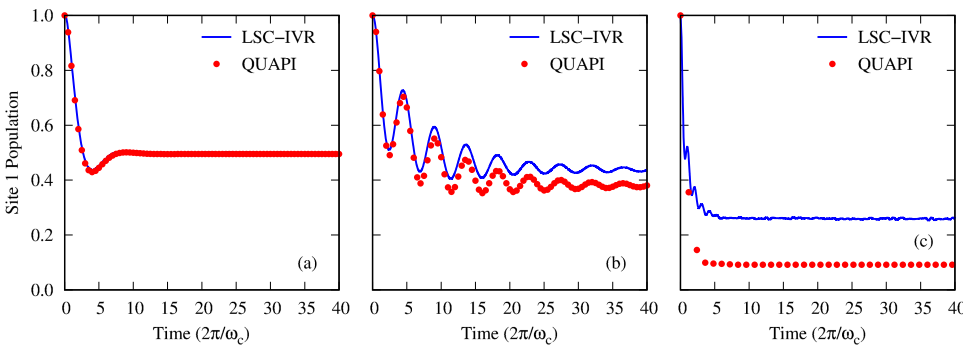


FIG. 1. Population dynamics calculated from the LSC-IVR method (blue line) and the numerically exact QUAPI method (red dots). We plot the population at site 1 as a function of time. Parameters used here: (a) $\Delta/\omega_c = 0.1$, $J/\omega_c = 0.5$, $\gamma = 0.2/\pi$, $k_B T/\omega_c = 10.0$; (b) $\Delta/\omega_c = 0.5$, $J/\omega_c = 0.5$, $\gamma = 0.2/\pi$, $k_B T/\omega_c = 2.0$; (c) $\Delta/\omega_c = 2.0$, $J/\omega_c = 2.0$, $\gamma = 2.0/\pi$, $k_B T/\omega_c = 0.5$.

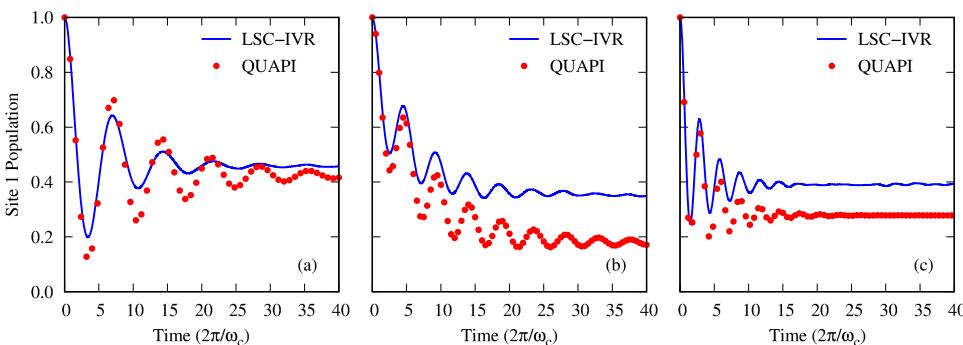


FIG. 2. Population dynamics calculated from the LSC-IVR method (blue line) and the numerically exact QUAPI method (red dots) at different eigen-energy gaps. (a) $\Delta E/\omega_c = 1.02$, (b) $\Delta E/\omega_c = 1.41$, (c) $\Delta E/\omega_c = 2.24$. The other parameters are $\gamma = 0.5/\pi$ and $k_B T/\omega_c = 0.5$, representative of the weak system-bath coupling and low temperature regime.

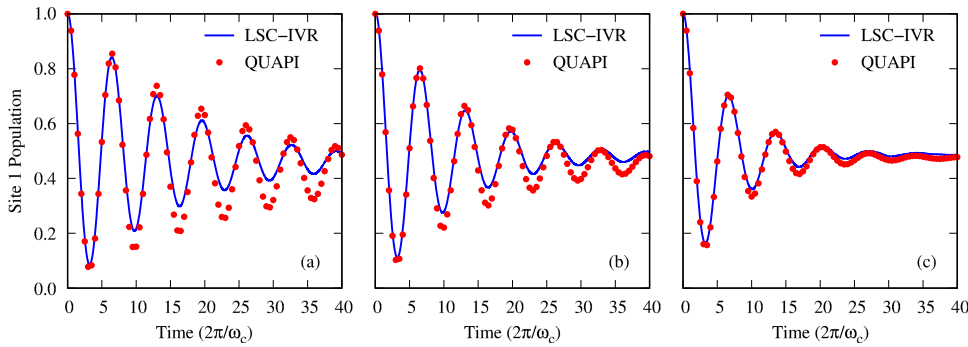


FIG. 3. Temperature dependent dynamics calculated from the LSC-IVR method (blue line) and the numerically exact QUAPI method (red dots). We plot the population at site 1 as a function of time at different temperatures: (a) $k_B T / \omega_c = 0.5$, (b) $k_B T / \omega_c = 1.0$, (c) $k_B T / \omega_c = 2.0$. Other parameters are $\Delta / \omega_c = 0.1$, $J / \omega_c = 0.5$, and $\gamma = 0.2 / \pi$.

In a fully quantum representation, these modes should not be directly involved in the energy transfer processes because their mode frequencies exceed the energy gap of the electronic system.

Moreover, we explore how the accuracy of the LSC-IVR method depends on the temperature. Figure 3 shows LSC-IVR dynamics at different temperatures. In Fig. 3, we observe that with the increase of the temperature from $k_B T / \omega_c = 0.5$ to 2.0, both the decoherence rate and the equilibrium population become more accurately described by the LSC-IVR approach, even in the small $\Delta E / \omega_c$ regime. As expected, in the high temperature case, the errors from the classical approximations become negligible. In addition, the LSC-IVR approach provides accurate oscillation frequencies, even in the low temperature cases (Fig. 3(a)). This indicates that even with the linearized semiclassical propagator, the LSC-IVR method provides accurate description of population beating dynamics for EET problems, leading to an appropriate approach for calculating quantum dynamics and spectral properties in condensed-phase systems.

Finally, we focus on the effects of the system-bath coupling strength γ on the performance of the LSC-IVR method. In Fig. 4, results with different system-bath coupling strengths (γ) are presented. We found that the LSC-IVR approach in general overestimates the decoherence rate in the large γ regime. Note that in the limit of zero system-bath coupling γ , the total system can be considered as $2 + N_b$ independent harmonic oscillators written in the MMST representation. In this situation, the analytic solution of the population at site 1 can be easily obtained in the LSC-IVR method, and it actually yields the exact result. However, as the coupling strength γ increases, errors from treating the bath position/momentum

operators as classical continuous variables increase, making the approach deviate from quantum results and leading to overestimation of decoherence rates. Note that in the limit of zero electronic couplings ($J = 0$), the Hamiltonian describes a pure-dephasing model, and the LSC-IVR is also exact in this case.

In summary, despite the incorrect equilibrium populations in most conditions and overestimated decoherence rates in some cases, the LSC-IVR method always yields correct oscillating frequencies in all parameter regime studied in this work. Moreover, the rates of the population transfer calculated by the LSC-IVR method are in excellent agreement with those from the QUAPI method, which motivates us to propose a long time limit correction algorithm to improve the performance of the LSC-IVR approach.

IV. LONG TIME CORRECTION

Our investigation of the accuracy of the LSC-IVR method for EET dynamics presented in Sec. III indicates that the major shortcoming of the LSC-IVR approach in simulating EET dynamics is the violation of detailed balance, which leads to incorrect equilibrium populations. To apply the LSC-IVR approach appropriately, we can either concentrate on models where the correct long time populations can be reproduced in the classical limit (e.g., a pure-dephasing system or a symmetric dimer system) or we should aim to amend this incorrect long-time limit. In this work, we propose to fix this shortcoming by using a post-processing algorithm to enforce that the equilibrium populations do satisfy the zeroth order equilibrium determined by the Boltzmann distribution according to the electronic Hamiltonian H_s .

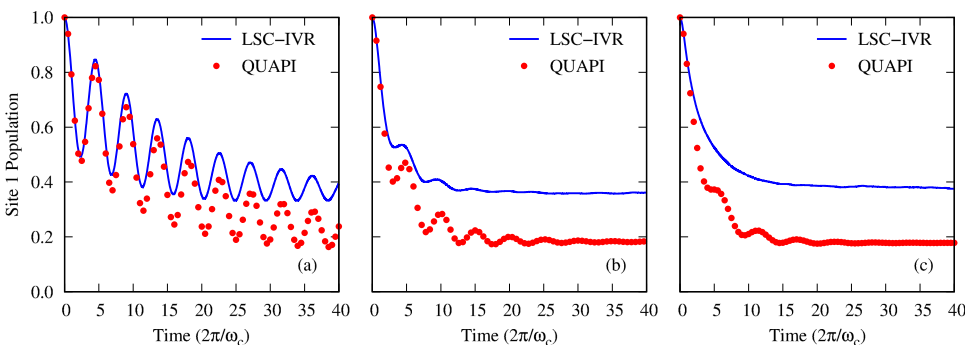


FIG. 4. Dynamics calculated from the LSC-IVR method (blue line) and the numerically exact QUAPI method (red dots) at different system-bath coupling strengths: (a) $\gamma / \pi = 0.2$, (b) $\gamma / \pi = 1.0$, (c) $\gamma / \pi = 2.0$. Other three parameters are $\Delta / \omega_c = 0.5$, $J / \omega_c = 0.5$, and $k_B T / \omega_c = 0.5$.

To this end, we aim specifically to make corrections to the long-time, incoherent dynamics, and the correction should leave the short-time dynamics along as accurate (or inaccurate) as before the correction. Therefore, we propose to use a correcting function to shift the longtime populations back to the proper equilibrium values. Given the time-dependent population at each site calculated by the LSC-IVR method, $P_n^{\text{LSC-IVR}}(t)$, we aim to compute a corrected population for each site, $P'_n(t)$, that will approach the estimated equilibrium population $P_n^{\text{eq}} = \langle n | e^{-\beta H_s} | n \rangle / Z$ at the longtime limit. We assume that $P'_n(t)$ can be computed from a correcting function $l_n(t)$,

$$P'_n(t) = P_n^{\text{LSC-IVR}}(t) - l_n(t). \quad (17)$$

The functional form of $l_n(t)$ is not important as long as it correctly shifts the equilibrium position at the long-time limit, while at the short and intermediate times it preserves dynamics given by the LSC-IVR method. This could be achieved by an exponential function of the following form:

$$l_n(t) = \left[P_n^{\text{LSC-IVR}}(\infty) - P_n^{\text{eq}} \right] (1 - e^{-\kappa_n t}), \quad (18)$$

where $P_n^{\text{LSC-IVR}}(\infty)$ is the long-time population given by the LSC-IVR method, and κ_n is an adjustable dynamical factor that controls the effective time scale of the correction. Note that $l_n(t)$ vanishes at the high temperature limit. Moreover, the long time limit of the LSC-IVR method cannot be obtained directly from the equations of motion, consequently we need to propagate the dynamics to obtain $P_n^{\text{LSC-IVR}}(\infty)$. Here, κ_n should be chosen such that the original population decay and decoherence rates given by the LSC-IVR method would not be affected. Therefore, we consider the relaxation time obtained from the LSC-IVR method

$$\tau_n = \frac{1}{P_n^{\text{LSC-IVR}}(0) - P_n^{\text{LSC-IVR}}(\infty)} \times \int_0^\infty \left[P_n^{\text{LSC-IVR}}(t) - P_n^{\text{LSC-IVR}}(\infty) \right] dt, \quad (19)$$

where τ_n represents the time scale of population relaxation predicted by the LSC-IVR method, and we argue that κ_n should be proportional to τ_n . Additional factors influence that population rates should also be included in the exponent κ_n ; hence, we conjecture that the exponent should be dependent on the system-bath coupling strength γ . After a systematic benchmark study, we find that $\kappa_n = \gamma/\tau_n$ yields excellent results when compared with the QUAPI results in most parameter regime studied in this work.

In this work, we estimate the equilibrium population using the Boltzmann distribution according to the zeroth order electronic Hamiltonian $P_n^{\text{eq}} = \langle n | e^{-\beta H_s} | n \rangle / Z$. Note that even more accurate long time populations could be achieved by the imaginary time path integral method,⁴¹ but the consequences will be negligible in the parameter regimes examined in this work. As a result, we limit our approach to corrections for the zeroth order equilibrium.

Figure 5 shows the corrected dynamics for models with the most severe long time limit problems in Sec. III. Clearly, the equilibrium populations are prominently revamped by using the *ad hoc* post-processing algorithm. It is interesting to note that with the long-time correction, the LSC-IVR method actually captures the short-time population beating dynamics quite well in a broad range of EET parameters studied here, as indicated in the nicely reproduced oscillation frequencies and dephasing times. This means that in the EET parameter space investigated in this work, the unphysical energy flow caused by the zero-point energy problem is mostly incoherent in nature. Note that we do not infer that the long-time correction also improves the short-time dynamics; the correction only shifts the population decay curve to exhibit a better comparison to the exact results.

In order to further examine the effectiveness of the LSC-IVR method with the long time correction, we provide additional results in Fig. 6 for parameter regimes that cause difficulties for perturbative methods. First we focus on the weak system-bath coupling regime with $\gamma = 0.2/\pi$ (Figs. 6(a) and 6(b)), where the LSC-IVR method with the long time correction yields excellent results. Note that Fig. 6(b) represents the situation in which the exciton energy gap exceeds the bath cutoff frequency. In this regime, the small polaron quantum master equation (SPQME) breaks down since the theory enforces a full displacement of bath coordinates to excited state vibrational equilibrium, whereas the slow bath modes should be more appropriately described by a partially displaced representation.⁴²

Moreover, we examine the strong electronic coupling regime ($J/\omega_c = 2.0$) where the electronic coherence is dominant. At a weak system-bath coupling strength (Fig. 6(c)), the LSC-IVR method with long time correction performs extremely well. Nevertheless, at a strong system-bath electronic coupling regime (Fig. 6(d)), the classical approximations still have effect on the decoherence time scale. The small deviation in the long time limit to the exact result is caused by the estimation of equilibrium population from the zeroth

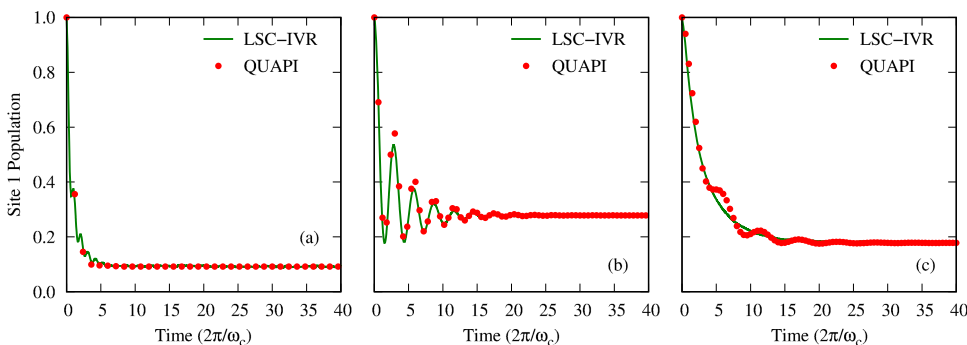


FIG. 5. Population dynamics calculated from the LSC-IVR method with the long time correction (green line) and the QUAPI method (red dots). The corresponding LSC-IVR results without the long time correction are shown in (a) Fig. 1(c), (b) Fig. 2(c), and (c) Fig. 4(c).

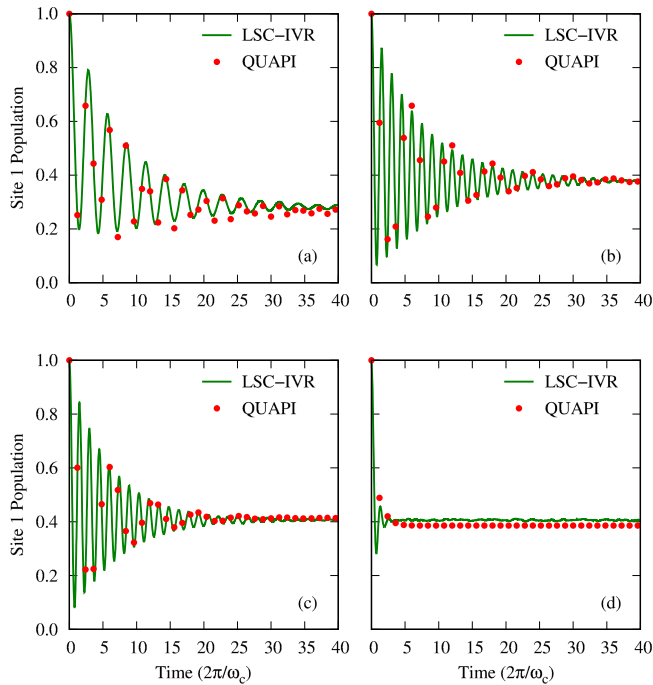


FIG. 6. Population dynamics calculated from the LSC-IVR method with the long-time correction (green line) and the QUAPI method (red dots). (a) and (b) are in the weak system-bath coupling regime ($\gamma = 0.2/\pi$), where the other parameters are set as follows: (a) $\Delta/\omega_c = 0.5$, $J/\omega_c = 1.0$, $k_B T/\omega_c = 0.5$; (b) $\Delta/\omega_c = 0.5$, $J/\omega_c = 2.0$, $k_B T/\omega_c = 0.5$. (c) and (d) are in the strong electronic coupling regime ($J/\omega_c = 2.0$), where the other parameters are set as follows: (c) $\Delta/\omega_c = 0.5$, $\gamma = 0.2/\pi$, $k_B T/\omega_c = 2.0$; (d) $\Delta/\omega_c = 0.5$, $\gamma = 2.0/\pi$, $k_B T/\omega_c = 2.0$.

order exciton Hamiltonian, which neglects shifts in equilibrium caused by the system-bath interactions. Notice that this regime also causes difficulty for the SPQME method due to the slow bath dynamics.⁴²

In addition, we benchmark the performance of the LSC-IVR approach at the weak electronic coupling regime ($J/\omega_c = 0.5$). Figure 7 shows that the LSC-IVR method with the long-time correction provides excellent results in this parameter regime. Note that in this regime, the coherent modified Redfield theory (CMRT) is not applicable.^{43,44} Since the CMRT is a perturbative method based on the exciton basis, it overestimates the coherence in this regime due to the neglect of the dynamical localization.

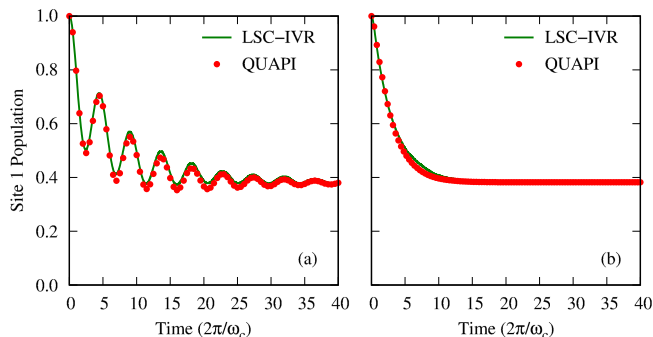


FIG. 7. Population dynamics calculated from the LSC-IVR method with the long time correction (green line) and the QUAPI method (red dots). We plot the population at site 1 as a function of time at the weak electronic coupling regime ($J/\omega_c = 0.5$). Other parameters are as follows: (a) $\Delta/\omega_c = 0.5$, $\gamma = 0.2/\pi$, and $k_B T/\omega_c = 2.0$; (b) $\Delta/\omega_c = 0.5$, $\gamma = 2.0/\pi$, and $k_B T/\omega_c = 2.0$.

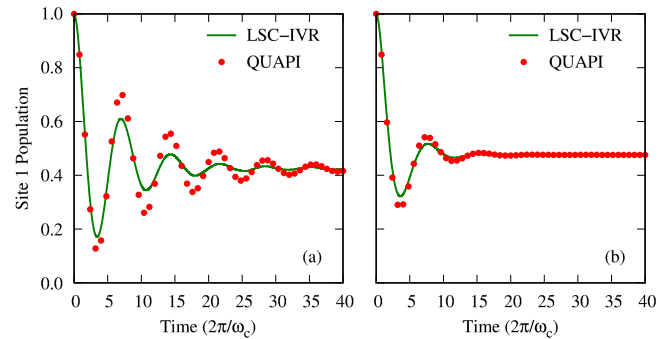


FIG. 8. Population dynamics calculated from the LSC-IVR in method with the long time correction (green line) and the QUAPI method (red dots). We plot the population at site 1 as a function of time for systems with a small excitonic energy gap ($\Delta/\omega_c = 0.1$, $J/\omega_c = 0.5$) at different temperatures as follows: (a) $k_B T/\omega_c = 0.5$, (b) $k_B T/\omega_c = 2.0$. The system-bath coupling strength is set as $\gamma = 0.5/\pi$.

Finally we analyze the influence of the temperature at a small excitonic energy gap regime ($\Delta/\omega_c = 0.5$, $J/\omega_c = 0.5$). In this regime, the accuracy of the LSC-IVR method declines (Fig. 8). At a low temperature (Fig. 8(a)), the quantum effect is dominant and the LSC-IVR method with long time correction underestimates the decoherence time. However, when the temperature increases, the error caused from the classical approximations can be alleviated (Fig. 8(b)). From the results in this section, we conclude that the applicable parameter range of the LSC-IVR seems to exceed that of several popular perturbative methods such as the small-polaron approach and the modified Redfield theory.

V. FMO DYNAMICS

To demonstrate that the LSC-IVR method with long-time correction is not limited to dimer systems, we apply the LSC-IVR method to simulate EET dynamics in the photosynthetic FMO complex. The FMO complex is a well-studied pigment-protein complex with a high-quality structure and effective Hamiltonian.^{45,46} It is composed of three identical subunits arranged in a three-fold symmetry and each of them contains seven or eight bacteriochlorophyll a (Bchl a) pigments embedded in a protein environment. The FMO complex conducts energy from the chlorosome light-harvesting antenna to the reaction center in the photosynthetic units of the green sulfur bacteria, and it has become a very popular model for the study of EET on the photosynthetic complex because of its remarkable near unity quantum efficiency.

We adopt the model for the FMO complex utilized in Ishizaki and Fleming's work.⁴⁷ The details of the model are described in the Appendix. To demonstrate the simulation of population beating dynamics, we focus on the low temperature case, $T = 77$ K, and assume that site 1 is initially excited. We use 300 000 trajectories in the LSC-IVR sampling for convergent results.

We first compare the population dynamics obtained from the original LSC-IVR method and those calculated by the hierarchy equation of motion (HEOM) approach^{48,49} in Fig. 9(a). We observe that both the oscillating frequencies and dephasing times are excellently reproduced by the LSC-IVR approach at all the sites. However, within the time scale relevant to

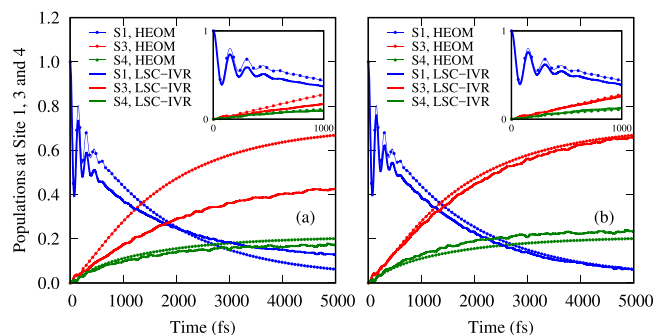


FIG. 9. Population dynamics of the FMO complex calculated from the LSC-IVR method (solid lines) and the HEOM method (dash-dot lines). (a) Original LSC-IVR without the long-time correction, (b) LSC-IVR with the long-time correction. For simplicity, we only show the results of sites 1, 3, and 4.

the EET process in the FMO complex, significant discrepancies between the LSC-IVR population dynamics and the exact results can be clearly seen, indicating serious problems in the long time limit of the LSC-IVR approach. As a result, we further apply the long time correction method proposed in Sec. IV to this model using the expected equilibrium populations estimated from the Boltzmann distribution of the system part (Fig. 9(b)). One should notice that since the τ_n 's are different for each site, the direct application of Eq. (18) will lead to non-conserved total population. We therefore renormalize the total population to unity in each step of the dynamical propagation. We observe that the correction makes minor effect on the population at the site 4 but significantly mitigates problems at sites 1 and 3. Clearly, the simple correction to the long-time limit significantly improved the performance of the LSC-IVR method in simulating EET dynamics in photosynthetic systems. Finally, we note that Tao and Miller have investigated the same model for EET dynamics in the FMO complex using the LSC-IVR method.³² Compared to their results, our LSC-IVR calculation with the aid of the long-time correction method provides much improved accuracy as demonstrated by our benchmark against the numerically exact HEOM data.

VI. CONCLUSION

In this work, we systematically investigated the accuracy of the LSC-IVR method in simulating EET dynamics of molecular aggregates. To this end, we benchmark the EET dynamics of a dimer system calculated by the LSC-IVR method against the dynamics simulated by the numerically exact QUAPI approach in a broad parameter regime. We reveal that the LSC-IVR method captures correct population beating dynamics and decoherence rates; however, the equilibrium populations obtained from the LSC-IVR method are often incorrect. Generally speaking, the deviations of LSC-IVR from the exact results can be explained by the violation of detailed balance due to the classical approximations made in the approach. It is also worthwhile to mention that the LSC-IVR method provides accurate transfer rates which are often the observables directly linked to experimental results. In this regard, LSC-IVR approach should provide an excellent rate theory for EET dynamics.

The problem of incorrect equilibrium populations can be largely removed by considering a post-processing algorithm

that applies exponential correction to the long-time dynamics to ensure equilibrium populations satisfying a Boltzmann distribution according to the zeroth-order electronic Hamiltonian. From a comprehensive benchmark, we find that the LSC-IVR method with this long-time correction provides excellent results in a wide range of EET parameters. In summary, we conclude that the LSC-IVR approach exhibits an applicable range that is broader than either the SPQME or CMRT approach. Finally, we utilize the LSC-IVR approach to simulate the EET dynamics in a representative photosynthesis complex, the FMO complex. When the long-time correction is applied, the LSC-IVR results are in excellent agreement with the numerically exact HEOM data.

It is noteworthy that while our work focuses on a correction to the long-time dynamics, a systematic approach to improve the short time dynamics that also partially corrects the long-time dynamics had been proposed and tested by Golosov and Reichman.²³ Furthermore, recently Cotton and Miller have proposed to utilize a symmetrical quasi-classical (SQC) windowing model to provide proper quantization of the electronic states in the MMST representation.^{50,51} This new approach has the same form as the LSC-IVR approach, but correctly treats the detailed balance in nonadiabatic dynamics by enforcing correct quantization conditions using a histogram window function, as have been demonstrated in asymmetric spin-boson problems⁵² and EET problems.⁵³ It will be interesting to benchmark the applicability of the SQC method in a broad EET parameter space, as we have demonstrated for the simple LSC-IVR method in this work. Nevertheless, given that the LSC-IVR and related methods are still quite popular in simulating quantum dynamical processes, we believe that the benchmark and physical insights presented in this work will be useful for more general applications of semiclassical methods to EET problems.

Notice that the LSC-IVR is exact in the high-temperature limit as well as the harmonic limit. The success of the LSC-IVR method in applications to EET dynamics in photosynthetic systems illustrates the strength of semiclassical methods in simulations of harmonic dynamics (in this case, the baths are harmonic), and we expect such semiclassical approaches could find broad applications by providing accurate and efficient means to simulate dynamical properties of similar spin-boson-like systems. Furthermore, since the LSC-IVR approach utilizes classical trajectories to describe the influence of the bath environments on the electronic sub-system, in principle, there will be no additional overhead to incorporate more general bath conditions such as correlated baths,³⁴ non-harmonic baths, or even realistic bath dynamics obtained from molecular dynamics simulations.⁵⁴⁻⁵⁷ We conclude that with the aid of the long-time correction algorithm proposed here, the LSC-IVR approach could be a powerful addition to our theoretical arsenal for simulating EET dynamics in molecular aggregates.

ACKNOWLEDGMENTS

Y.C.C. thanks the Ministry of Science and Technology, Taiwan (Grant No. NSC 105-2113-M-002-012), National Taiwan University (Grant No. 103R891305), and Center for Quantum Science and Engineering (Subproject

No. 103R891401) for financial support. We are grateful to Computer and Information Networking Center, National Taiwan University for the support of high-performance computing facilities. We are grateful to the National Center for High-Performance Computing for computer time and facilities. Y.C.C. thanks Professor Qiang Shi for kindly providing us the HEOM data on FMO dynamics.

APPENDIX: MODEL FMO HAMILTONIAN

The model utilized for describing the EET dynamics in the photosynthetic FMO complex is taken from Ishizaki and Fleming.⁴⁷ The Hamiltonian reads

$$H_{\text{FMO}} = \begin{pmatrix} 300.0 & -87.7 & 5.5 & -5.9 & 6.7 & -13.7 & -9.9 \\ -87.7 & 420.0 & 30.8 & 8.2 & 0.7 & 11.8 & 4.3 \\ 5.5 & 30.8 & 100.0 & -53.5 & -2.2 & -9.6 & 6.0 \\ -5.9 & 8.2 & -53.5 & 210.0 & -70.7 & -17.0 & -63.3 \\ 6.7 & 0.7 & -2.2 & -70.7 & 370.0 & 81.1 & -1.3 \\ -13.7 & 11.8 & -9.6 & -17.0 & 81.1 & 520.0 & 39.7 \\ -9.9 & 4.3 & 6.0 & -63.3 & -1.3 & 39.7 & 330.0 \end{pmatrix}. \quad (\text{A1})$$

The spectral density function used in the model describes an over-damped Brownian oscillator expressed in the Drude-Lorentz form

$$\mathcal{J}^B(\omega) = 2\lambda\omega\gamma/(\omega^2 + \gamma^2), \quad (\text{A2})$$

and it can be discretized by the same procedure described in Sec. II D. Following Ishizaki and Fleming, we set the reorganization energy λ and the bath relaxation rate γ as 35 cm^{-1} and $1/50 \text{ fs}^{-1}$, respectively. To simulate the spectral density using discrete harmonic modes, we use 200 bath modes coupled to each site in our LSC-IVR calculations.

¹J. C. Tully, *Faraday Discuss.* **110**, 407 (1998).

²J. E. Subotnik and N. Shenvi, *J. Chem. Phys.* **134**, 024105 (2011).

³R. Kapral, *Annu. Rev. Phys. Chem.* **57**, 129 (2006).

⁴S. Bai, W. Xie, and Q. Shi, *J. Phys. Chem. A* **118**, 9262 (2014).

⁵I. R. Craig and D. E. Manolopoulos, *J. Chem. Phys.* **121**, 3368 (2004).

⁶S. Habershon, D. E. Manolopoulos, T. E. Markland, and T. F. Miller III, *Annu. Rev. Phys. Chem.* **64**, 387 (2013).

⁷J. E. Subotnik, A. Jain, B. Landry, A. Petit, W. Ouyang, and N. Bellonzi, *Annu. Rev. Phys. Chem.* **67**, 387 (2016).

⁸W. Xie, S. Bai, L. Zhu, and Q. Shi, *J. Phys. Chem. A* **117**, 6196 (2013).

⁹J. H. V. Vleck, *Proc. Natl. Acad. Sci. U. S. A.* **14**, 178 (1928).

¹⁰X. Sun, H. Wang, and W. H. Miller, *J. Chem. Phys.* **109**, 7064 (1998).

¹¹W. H. Miller, *J. Phys. Chem. A* **105**, 2942 (2001).

¹²W. H. Miller, *Proc. Natl. Acad. Sci. U. S. A.* **102**, 6660 (2005).

¹³H.-D. Meyer and W. H. Miller, *J. Chem. Phys.* **70**, 3214 (1979).

¹⁴G. Stock and M. Thoss, *Phys. Rev. Lett.* **78**, 578 (1997).

¹⁵M. Thoss and G. Stock, *Phys. Rev. A* **59**, 64 (1999).

¹⁶N. Makri and K. Thompson, *Chem. Phys. Lett.* **291**, 101 (1998).

¹⁷K. Thompson and N. Makri, *J. Chem. Phys.* **110**, 1343 (1999).

¹⁸H. Wang, X. Sun, and W. H. Miller, *J. Chem. Phys.* **108**, 9726 (1998).

¹⁹J. Liu, *Int. J. Quantum Chem.* **115**, 657 (2015).

²⁰N. Ananth, C. Venkataraman, and W. H. Miller, *J. Chem. Phys.* **127**, 084114 (2007).

²¹H. Wang, X. Song, D. Chandler, and W. H. Miller, *J. Chem. Phys.* **110**, 4828 (1999).

²²G. Stock and U. Muller, *J. Chem. Phys.* **111**, 65 (1999).

²³A. A. Golosov and D. R. Reichman, *J. Chem. Phys.* **114**, 1065 (2001).

²⁴W. H. Miller, *J. Chem. Phys.* **136**, 210901 (2012).

²⁵X. Sun, H. Wang, and W. H. Miller, *J. Chem. Phys.* **109**, 4190 (1998).

²⁶Q. Shi and E. Geva, *J. Phys. Chem. A* **107**, 9059 (2003).

²⁷J. Liu and W. H. Miller, *J. Chem. Phys.* **134**, 104101 (2011).

²⁸J. Liu and W. H. Miller, *J. Chem. Phys.* **134**, 104102 (2011).

²⁹G. S. Engel, T. R. Calhoun, E. L. Read, T. K. Ahn, T. Mancal, Y.-C. Cheng, R. E. Blankenship, and G. R. Fleming, *Nature* **446**, 782 (2007).

³⁰H. Lee, Y.-C. Cheng, and G. R. Fleming, *Science* **316**, 1462 (2007).

³¹Y.-C. Cheng and G. R. Fleming, *Annu. Rev. Phys. Chem.* **60**, 241 (2009).

³²G. Tao and W. H. Miller, *J. Phys. Chem. Lett.* **1**, 891 (2010).

³³P. Huo and D. F. Coker, *J. Chem. Phys.* **133**, 184108 (2010).

³⁴P. Huo and D. F. Coker, *J. Chem. Phys.* **136**, 115102 (2012).

³⁵L. A. Pachon and P. Brumer, *Phys. Chem. Chem. Phys.* **14**, 10094 (2012).

³⁶N. Makri and D. E. Makarov, *J. Chem. Phys.* **102**, 4600 (1995).

³⁷N. Makri and M. Topaler, *Chem. Phys. Lett.* **210**, 285 (1993).

³⁸R. Kubo and M. Toda, *Statistical Physics II: Nonequilibrium Statistical Mechanics*, 2nd ed. (Springer, 1998).

³⁹U. Muller and G. Stock, *J. Chem. Phys.* **111**, 77 (1999).

⁴⁰T. Renger, V. May, and O. Kühn, *Phys. Rep.* **343**, 137 (2001).

⁴¹N. Makri, *Comput. Phys. Commun.* **63**, 389 (1991).

⁴²H.-T. Chang, P.-P. Zhang, and Y.-C. Cheng, *J. Chem. Phys.* **139**, 224112 (2013).

⁴³Y.-H. Hwang-Fu, W. Chen, and Y.-C. Cheng, *Chem. Phys.* **447**, 46 (2015).

⁴⁴Y. Chang and Y.-C. Cheng, *J. Chem. Phys.* **142**, 034109 (2015).

⁴⁵R. E. Fenna and B. W. Matthews, *Nature* **258**, 573 (1975).

⁴⁶D. E. Tronrud, J. Wen, L. Gay, and R. E. Blankenship, *Photosynth. Res.* **100**, 79 (2009).

⁴⁷A. Ishizaki and G. R. Fleming, *Proc. Natl. Acad. Sci. U. S. A.* **106**, 17255 (2009).

⁴⁸R. Kubo and Y. Tanimura, *J. Phys. Soc. Jpn.* **58**, 101 (1989).

⁴⁹L. Chen, R. Zheng, Y. Jing, and Q. Shi, *J. Chem. Phys.* **134**, 194508 (2011).

⁵⁰S. J. Cotton and W. H. Miller, *J. Phys. Chem. A* **119**, 12138 (2015).

⁵¹W. H. Miller and S. J. Cotton, *Faraday Discuss.* **195**, 9 (2016).

⁵²S. J. Cotton and W. H. Miller, *J. Chem. Phys.* **145**, 144108 (2016).

⁵³S. J. Cotton and W. H. Miller, *J. Chem. Theory Comput.* **12**, 983 (2016).

⁵⁴C. Olbrich, J. Struempfer, K. Schulten, and U. Kleinekathöfer, *J. Phys. Chem. Lett.* **2**, 1771 (2011).

⁵⁵Y. Jing, R. Zheng, H.-X. Li, and Q. Shi, *J. Phys. Chem. B* **116**, 1164 (2012).

⁵⁶L. Zhang, D.-A. Silva, H. Zhang, A. Yue, Y. Yan, and X. Huang, *Nat. Commun.* **5**, 4170 (2014).

⁵⁷S. Chandrasekaran, M. Aghtar, S. Valteau, A. Aspuru-Guzik, and U. Kleinekathöfer, *J. Phys. Chem. B* **119**, 9995 (2015).